Laser Physics, Vol. 12, No. 1, 2002, pp. 21–36.

Dynamics of Trapped Bose–Einstein Condensates: Beyond the Mean-Field

M. K. Olsen[1], L. I. Plimak[1], V. I. Kruglov[1], J. J. Hope[2], P. D. Drummond[3], and M. J. Collett[1]

[1] *Department of Physics, University of Auckland, Private Bag, Auckland, 92019 New Zealand*
e-mail: l.plimak@auckland.ac.nz

[2] *Department of Physics and Theoretical Physics, The Australian National University, Canberra, Australian Capital Territory, 0200 Australia*

[3] *Department of Physics, The University of Queensland, St. Lucia, Queensland, 4072 Australia*

Received May 10, 2001

Abstract—Since dilute Bose gas condensates were first experimentally produced, the Gross–Pitaevskii equation has been successfully used as a descriptive tool. As a mean-field equation, it cannot by definition predict anything about the many-body quantum statistics of condensate. We show here that there are a class of dynamical systems where it cannot even make successful predictions about the mean-field behavior, starting with the process of evaporative cooling by which condensates are formed. Among others are parametric processes, such as photoassociation and dissociation of atomic and molecular condensates.

1. INTRODUCTION

One of the remarkable predictions of quantum mechanics is the Bose–Einstein condensation of indistinguishable particles. At sufficiently low temperatures the ground state of a system can become macroscopically occupied, with quantum features being observable at the macroscopic level [1–3]. Dilute alkali gas Bose–Einstein condensation (BEC) was first observed in the laboratory in the last decade of the previous millennium [4] and has since been reproduced by a number of workers in the field. Theoretical investigations of BEC, especially where the dynamics are concerned, have largely used the Gross–Pitaevskii equation (GPE) [5] and have been remarkably successful. However, even though it is derived from quantum statistical considerations, the GPE cannot be used to calculate quantum statistical properties of BEC. As an equation of motion for the condensate mean-field, or even for the Hartree–Fock many particle wavefunction of the BEC, it may be expected that it would accurately describe the dynamical behavior of the condensate mean field. In this article we review a number of instances where it cannot even do this successfully.

As with many problems, there is more than one way to go beyond the mean-field approximation. Even at zero temperature, where thermal effects are non-existent, the condensate is influenced by quantum noise, which in principle can be fully modelled using a functional positive-P representation or partially modelled using a truncated functional Wigner representation [6–9]. The use of the positive-P representation, however, while exact, must be performed numerically and encounters huge stability problems with trapped condensates. The truncated Wigner, while stable, is equivalent to the semiclassical theory of stochastic electrodynamics [10] and is at best an approximate method.

Another method of going beyond the mean-field approach is to use the Hartree–Fock–Bogoliubov theory. As an illustration, we can consider the case of the resonant coupling between atomic and molecular condensates [11, 12] using either a Feshbach resonance or a Raman transition. In this case quantum correlations are thought to dominate below a critical density [13], which must be exceeded in order to observe mean-field "superchemistry" behavior. This is an experimentally significant point, since below the critical density, dynamical predictions are made which are at variance with those of the mean field model. The possibility of a phase transition [11] induced by quantum fluctuations is also interesting in this regard.

2. INCLUDING QUANTUM EFFECTS

Quantum correlations and fluctuations have been treated perturbatively in equilibrium weakly interacting Bose condensates, since the pioneering work of Bogoliubov [14], Huang [15], Beliaev [16] and others. These methods appear in many textbooks [17], and have been extended via the use of various approximations schemes that add quantum corrections to the mean-field equations [18]. In the one-dimensional case, there are even exact solutions [19] for the interacting ground-state and excited states. More general treatments of thermal equilibrium quantum effects in trapped condensates have relied on the use of Monte Carlo techniques [20].

By comparison, there have been relatively few attempts to treat quantum dynamics in BEC, and it is sometimes claimed that no computational approach is feasible [21], due to the large size of the many-body Hilbert space. The first published attempt to model dilute gas trapped BEC while rigorously including the

quantum features was by Steel *et al.* [6]. This work developed functional positive-*P* and Wigner representations for a trapped condensate, which were then used to calculate the first order coherence properties as a condensate evolved from an initial state. The motivation for this work was that, while a single mode model may give an estimate for the phase diffusion time [22] for example, it could never describe spatial coherence properties or the role of local density and phase fluctuations. Hence, there was a need for techniques to treat the quantum dynamics of the condensate using a fully spatially dependent field rather than a few mode approach.

Another motivation for treating BEC quantum mechanically comes by analogy with optical fibres. The propagation of the optical field in a nonlinear fibre is governed by what is known as a nonlinear Schrödinger equation which includes the effects of fibre dispersion and the Kerr nonlinearity of the medium [23, 24]. The Heisenberg field operator describing a BEC confined in a one-dimensional potential well obeys a strikingly similar equation to that of the fibre soliton system, differing only by the addition of the trapping potential and the interpretation of the dispersive term which in a condensate represents the kinetic energy. Both number and quadrature squeezing have been predicted and observed in soliton propagation in fibres [23–28] and, given that multi-mode quantum treatments proved essential for the accurate prediction of quantum soliton properties, it was reasonable to assume the same would hold true in Bose condensates. In fact, the nonlinearity occurring in the condensate problem is typically far larger than for the soliton case, and thus the role of quantum noise could be even more important.

A quantum calculation of the evolution of the BEC field operator is a formidable task as the Hilbert space for the system is truly vast. A direct route using a number state basis is not a realistic option, but techniques of quantum optics may be generalized to provide a complete description of the condensate field operator and any desired expectation value can, in principle, be calculated. The key to this approach is the representation of the density operator using phase-space quasi-probability functions. We will outline the derivation of the equations resulting from the use of a functional positive-*P* representation below.

2.1. One-Dimensional Trapped condensates

A one-dimensional system can be considered by assuming a highly anisotropic harmonic trap with the longitudinal and radial trap frequencies (ω_z and ω_r respectively) satisfying $\lambda = \omega_z/\omega_r \ll 1$. This corresponds to a cigar-shaped trap such as has commonly been used in experiments [29, 30]. With strong radial confinement, it can be assumed the nonlinearity plays a negligible role in the radial direction. The field operator is then assumed to factorize with its transverse dependence completely described by a coherent state occupation of the lowest mode of the trap. The Heisenberg field operator then has the form

$$\hat{\Psi}(\mathbf{x}) = \left(\frac{m\omega_r}{\pi\hbar}\right)^{1/2} \exp\left(-\frac{m\omega_r r^2}{2\hbar}\right)\hat{\phi}(z, t). \tag{1}$$

Adopting harmonic oscillator units in the axial direction with $a_0 = \sqrt{\hbar/(m\omega_z)}$, $\tau = \omega_z t$, $x = z/a_0$ and $\hat{\psi}(x, \tau) = \sqrt{a_0}\hat{\phi}(z, t)$, the one-dimensional second-quantised Hamiltonian is (dropping the spatial dependence for notational convenience)

$$\hat{H} = \int_{-\infty}^{\infty} dx \hat{\psi}^\dagger \mathcal{K} \hat{\psi} + \frac{\Gamma}{2}\int_{-\infty}^{\infty} dx \hat{\psi}^\dagger \hat{\psi}^\dagger \hat{\psi}\hat{\psi}, \tag{2}$$

where $\mathcal{K}$ is the linear operator

$$\mathcal{K} = -\frac{1}{2}\frac{d^2}{dx^2} + \frac{1}{2}x^2 - \mu, \tag{3}$$

μ is the scaled chemical potential, and $\Gamma = 2a/(\lambda a_0)$ is the scaled nonlinear constant with a the *s*-wave scattering length.

A concise derivation of positive-*P* [31] field equations is obtained by introducing the functional *P*-distribution [32, 33]

$$P(\{\psi, \psi^*\}, \tau) = \rho^{(a)}(\{\hat{\psi}, \hat{\psi}^\dagger\}, \tau)\big|_{\hat{\psi}\to\psi, \hat{\psi}^\dagger\to\psi^*}, \tag{4}$$

where $\rho^{(a)}$ denotes the density operator $\rho(\tau)$ antinormally ordered with respect to the field-operators $\hat{\psi}$, $\hat{\psi}^\dagger$ in the Schrödinger picture. Putting the master equation obtained from the Hamiltonian (2) into antinormal order, and using the following functional analogues of the operator correspondences [34]

$$\begin{aligned}
\hat{\psi}\rho &\longleftrightarrow \psi P(\psi),\\
\hat{\psi}^\dagger\rho &\longleftrightarrow \left(\psi^* - \frac{\delta}{\delta\psi}\right)P(\psi),\\
\rho\hat{\psi} &\longleftrightarrow \left(\psi - \frac{\delta}{\delta\psi^*}\right)P(\psi),\\
\rho\hat{\psi}^\dagger &\longleftrightarrow \psi^* P(\psi),
\end{aligned} \tag{5}$$

one finds the functional Fokker–Planck equation,

$$\begin{aligned}
\frac{\partial P}{\partial\tau} = \int_{-\infty}^{\infty} dx \Bigg\{ &-\frac{\delta}{\delta\psi(x)}[-i(\mathcal{K}\psi(x) + \Gamma|\psi(x)|^2\psi(x))]\\
&+ \frac{\Gamma}{2}\frac{\delta^2}{\delta\psi^2(x)} i\psi^2(x)\Bigg\}P + \text{c.c.}
\end{aligned} \tag{6}$$

The diffusion matrix of this equation is non positive-definite and so there is no straightforward mapping

onto a single stochastic differential equation [34]. A positive-P representation [35] must be used, doubling the phase space with the mapping

$$\begin{aligned}\psi(x,t) &\longrightarrow \psi_1(x,t),\\ \psi^*(x,t) &\longrightarrow \psi_2^*(x,t),\end{aligned} \tag{7}$$

where $\psi_1(x,\ t)$ and $\psi_2(x,\ t)$ are independent fields. Sometimes the notation $\psi^+(x,\ t)$ is used instead of $\psi_2^*(x,t)$, to denote the c-number field that corresponds to $\hat{\psi}^\dagger$. We now obtain a positive-definite diffusion matrix and finally derive the pair of Itô stochastic differential equations,

$$\begin{aligned}i\partial_\tau\psi_1(x,\tau) &= \mathcal{H}\psi_1(x,\tau) + \Gamma\psi_2^*(x,\tau)\psi_1^2(x,\tau)\\ &\quad + \sqrt{i\Gamma}\psi_1(x,\tau)\eta_1(x,\tau),\\ i\partial_\tau\psi_2(x,\tau) &= \mathcal{H}\psi_2(x,\tau) + \Gamma\psi_1^*(x,\tau)\psi_2^2(x,\tau)\\ &\quad + \sqrt{i\Gamma}\psi_2(x,\tau)\eta_2(x,\tau),\end{aligned} \tag{8}$$

where the noise sources η_1 and η_2 are real, Gaussian and delta-correlated in time and space: $\overline{\eta_i(x,\tau)\eta_j(x',\tau')} = \delta_{ij}\delta(x-x')\delta(\tau-\tau')$. This set of coupled equations can then be numerically integrated on a spatial lattice and averaged over a large number of trajectories, a procedure which was first carried out for the optical soliton squeezing problem [36].

The positive-P representation gives exact results for as long as the ensemble averages converge. However, in the case of the condensate the trajectories are prone to large excursions from the mean which quickly cause the simulation to blow up. Such problems with the positive-P representation occur especially in systems with strong nonlinearity and weak (or vanishing) damping which is precisely the situation of a trapped interacting Bose condensate. Some alternative stochastic representations are being developed which promise to enable the accurate calculation of expectation values without the numerical instability problems of the usual positive-P [37–39]. However, as is demonstrated below, the positive-P has been used successfully to make some predictions of BEC dynamics beyond the mean-field model. A second problem with these numerical simulations is the need for an accurate understanding of the starting quantum-state in a simulation. As we shall see below, this has been treated to some extent by the numerical simulation of the cooling process itself.

3. EVAPORATIVE COOLING

The process of evaporative cooling which has been successfully used to produce BEC inside magneto-optic traps has no classical description. It is commonly described using kinetic methods, which discard the coherence properties found in the final state [40], although other phase-space methods have been proposed [41, 42]. The GPE approach starts with the condensate already made and can say nothing about the quantum state. Exact numerical phase-space methods have therefore been used for direct quantum dynamical calculations of the cooling and formation of BEC on a three-dimensional lattice [7]. The results were restricted to small condensates due to the large numbers of modes involved, but were very similar to what is observed experimentally. In particular, quantum evaporative cooling was found, followed by a clear transition to a condensate. This was strongly influenced by non-classical features of the quantum dynamics. The calculations also indicated additional structure, which was interpreted as spontaneous formation of vortices—a process of wide interest in other fields of physics [43]. These appeared to originate in the residual orbital angular momentum of the trapped atoms, which was neglected in previous studies, and would provide a significant test of the quantum theory.

In the calculations, 3×10^4 relevant modes were included, with up to 10^4 atoms present. The quantum state-vector therefore had over 10^{10000} components and was not amenable to quantum number state calculations in the time-domain. A more practical technique was to utilize the phase-space methods, namely the coherent-state (positive-P) phase-space equations which are exactly equivalent to the relevant quantum equations provided phase-space boundary terms [44] vanish.

The model used included the usual non-relativistic Hamiltonian for neutral atoms in a trapping potential $V(\mathbf{x})$, interacting via a potential $U(\mathbf{x})$, together with absorbing reservoirs $\hat{R}(\mathbf{x})$, in $d = 2$ or $d = 3$ dimensions,

$$\begin{aligned}\hat{H} &= \int d^d\mathbf{x}\Big[\frac{\hbar^2}{2m}\nabla\hat{\Psi}^\dagger(\mathbf{x})\nabla\hat{\Psi}(\mathbf{x}) + V(\mathbf{x})\hat{\Psi}^\dagger(\mathbf{x})\hat{\Psi}(\mathbf{x})\\ &\quad + \hat{\Psi}^\dagger(\mathbf{x})\hat{R}(\mathbf{x}) + \hat{\Psi}(\mathbf{x})\hat{R}^\dagger(\mathbf{x})\\ &\quad + \frac{1}{2}\int d^d\mathbf{y}\,U(\mathbf{x}-\mathbf{y})\hat{\Psi}^\dagger(\mathbf{x})\hat{\Psi}^\dagger(\mathbf{y})\hat{\Psi}(\mathbf{y})\hat{\Psi}(\mathbf{x})\Big].\end{aligned} \tag{9}$$

Here $\hat{R}(\mathbf{x})$ represents a localized absorber that removes the neutral atoms, for example via collisions with foreign atoms, or at the location of the "RF-scalpel" resonance, which is used to cause evaporative cooling. $\hat{\Psi}$ was expanded using free-field modes with a momentum cut-off $k_{\max}$. Provided that $k_{\max} \ll a_0^{-1}$, where a_0 is the S-wave scattering length, $U(\mathbf{x}-\mathbf{y})$ can be replaced by the renormalized pseudo-potential $u\delta^d(\mathbf{x}-\mathbf{y})$, where $u = 4\pi a_0\hbar^2/m$ in three dimensions. In two dimensions, u is defined similarly but with a factor ξ_0 in the denominator, which corresponds to the effective spatial extent of the condensate in the third direction. This factor is of the order of the lattice spacing in the simulations, and is chosen to be equal to x_0, the scaling length.

Following similar procedures to those of Section 2, the positive-*P* equations are found as

$$i\hbar\frac{\partial\psi_j}{\partial t} = \left[\frac{-\hbar^2}{2m}\nabla^2 + u\psi_j\psi^*_{3-j} + V(\mathbf{x}) - \frac{i\hbar}{2}\Gamma(\mathbf{x}) + \sqrt{i\hbar u}\xi_j(t,\mathbf{x})\right]\psi_j, \tag{10}$$

where $j = 1, 2$ and where the stochastic fields ψ_j are the coherent state amplitudes of a non-diagonal coherent state projector, $|\psi_1\rangle\langle\psi_2|/\langle\psi_2|\psi_1\rangle$. Quantum effects come from the terms ξ_j, which are real Gaussian stochastic fields, with the correlations:

$$\langle\xi_i(s,\mathbf{x})\xi_j(t,\mathbf{y})\rangle = \delta_{ij}\delta(s-t)\delta^d(\mathbf{x}-\mathbf{y}). \tag{11}$$

The form of the potentials was chosen to be

$$V(\mathbf{x},t) = (1-\alpha t)V_{\max}\sum_{j=1}^{d}[\sin(\pi x_j/L_j)]^2, \tag{12}$$

where α is typically the inverse of the total simulation time. The potential height was swept downwards linearly in time, thus successively removing cooler and cooler subpopulations of atoms. The absorption rate $\Gamma(\mathbf{x})$ was chosen as

$$\Gamma(\mathbf{x}) = \Gamma_{\max}\sum_{j=1}^{d}[\sin(\pi x_j/L_j)]^{50}. \tag{13}$$

Here L_j is the trap width in the j-th direction, such that $-L_j/2 \le x_j \le L_j/2$. The sinusoidal shape of the potential and absorption was chosen so that the trap would be harmonic near the center, and smoothly approach a maximum near the edge. Thus hot atoms were absorbed when they reached regions of large $\Gamma(\mathbf{x})$, located near the trap edges.

The results of the simulations depended critically on the exact parameters chosen, as expected from the known sensitivity of the experiments. It was necessary to consider rather small traps because the numerical lattice spacing used to sample the stochastic fields in x-space must be of order $\Delta x = 1/k_{\max}$, where $k_{\max}$ is the largest ordinary momentum considered in the problem. However, the value of the corresponding kinetic energy, $E_K = (\hbar k_{\max})^2/2m$, must be large enough to allow energetic atoms to escape, otherwise no cooling can take place. This set an upper-bound on the lattice spacing, and hence on the maximum trap size that could be computed (which depended on the number of lattice points). The trap sizes that could be treated had dimensions of the order of microns. The trap simulated had a width of $L_j = 10$ μm, with a potential height of $V_{\max}/k_B = 1.9 \times 10^{-7}$ K, and an initial temperature of $T_0 = 2.4 \times 10^{-7}$ K.

The initial atomic density must of course be such that the occupation of each momentum state cannot be greater than one, otherwise the starting point would already show condensation. This placed a limit on the number of atoms which could be simulated, assuming an initially non-condensed grand canonical ensemble of (approximately) non-interacting atoms. There were initially around 500 atoms in the two dimensional simulations, and 10000 in the three dimensional case, corresponding to atomic densities of $n_0 = 5.0 \times 10^{12}/\mathrm{m}^2$ and $n_0 = 1.0 \times 10^{19}/\mathrm{m}^3$ respectively.

It was found that the effect of the stochastic terms on the dynamics was very large. In fact the quantum fluctuations were much larger than the initial thermal fluctuations, such that the initial features of the distribution do not persist. This meant that the choice of the initial state of the system is not critical, and also that in order to determine properties of the final quantum ground state of the system, the stochastic terms are vital. Simulations done using the Gross–Pitaevskii equation, with initial conditions corresponding to a thermal state did not show strong Bose condensation effects. This demonstrated the highly non-classical nature of the early stages of Bose condensation, in which spontaneous transitions to the lowest energy states clearly play an important role.

For the simulations, $a_0 = 0.6$ nm and the mass, corresponding to rubidium, is $m = 1.5 \times 10^{-25}$ kg, corresponding to relatively weakly interacting atoms, in order to reduce the sampling error. The figures show results plotted in normalized units, with space scaled by $x_0 = 0.76$ μm, and time scaled by $t_0 = 0.79$ ms. The boundary absorption term was set to $\Gamma_{\max} \simeq 10^3\ \mathrm{s}^{-1}$. Figure 1 shows the ensemble average of 55 trajectories of the atomic density, $\langle n(k)\rangle$, in Fourier space for a two-dimensional simulation. It was found that the peak final momentum state population was much greater than one, the condensation effect being more pronounced in three dimensions. This demonstrated that the evaporative cooling process is more efficient with the extra degree of freedom and the greater number of atoms that were present.

Since the condensate does not have to form in the ground-state, the Bose-condensed peaks that occur at different momentum values in single runs were averaged out in the overall ensemble. A more useful indication of condensation is given by the following measure of phase-space confinement,

$$Q = \frac{\int d^3k\,\langle\psi_1(\mathbf{k})\psi_1(\mathbf{k})\psi_2^*(\mathbf{k})\psi_2^*(\mathbf{k})\rangle}{\left(\int d^3k\,\langle\psi_1(\mathbf{k})\psi_2^*(\mathbf{k})\rangle\right)^2 x_0^3}, \tag{14}$$

being the quantum analogue of the participation ratio defined by Hall [45]. Figure 2 shows the evolution of Q calculated from 15 runs of the three dimensional simulation. The sharp rise near $t = 100$ is a strong indication of condensation occurring at this point.

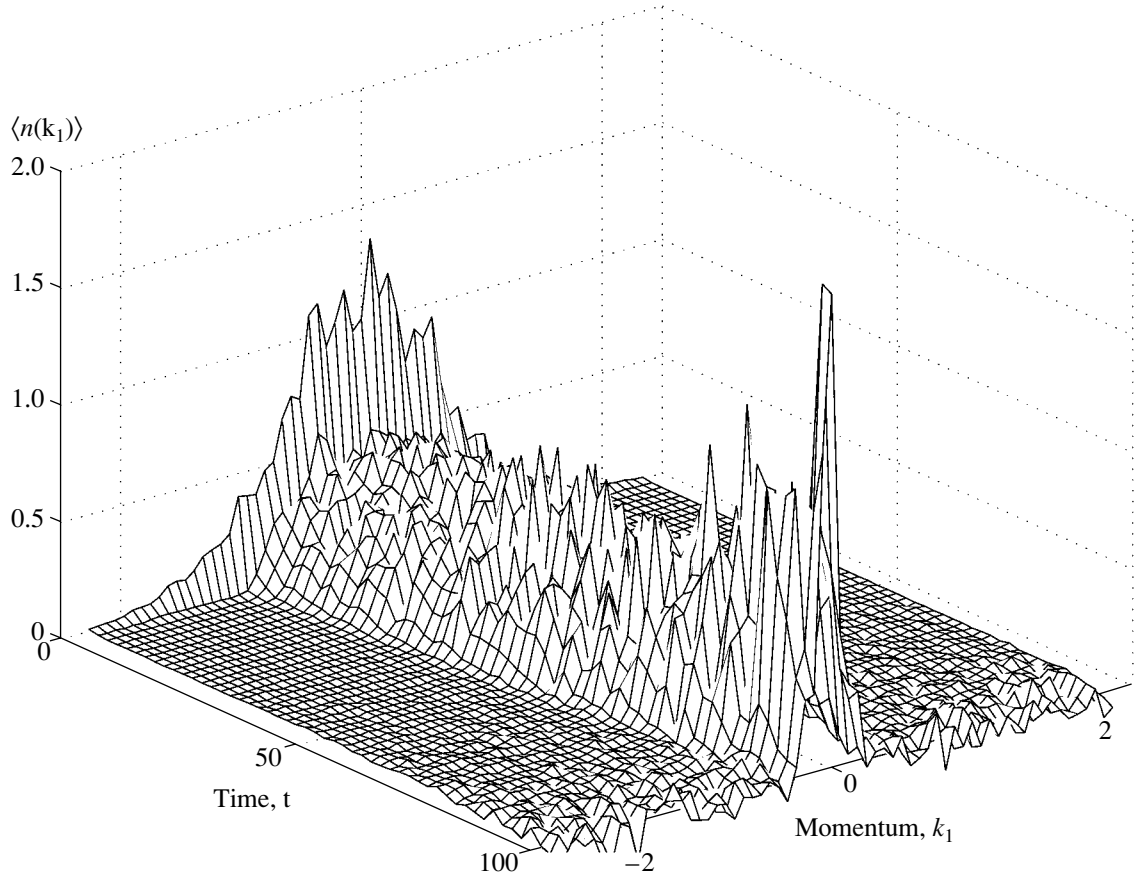

Fig. 1. Simulation of a two-dimensional Bose condensate, showing the ensemble average (55 paths) atom density $\langle n(k)\rangle$ along one dimension in Fourier space versus time.

Finite-size condensates in atom traps are not constrained to fall into the $J = 0$ angular momentum eigenstate. Both the initial and the escaping atoms have an arbitrary angular momentum. It can be estimated that the variance in angular momentum will scale approximately as $\langle \hat{J}^2 \rangle \propto N$, from central limit theorem arguments. The angular momentum can be carried either by quasi-particles or vortices, although a volume-filling jth order vortex has $J = Nj$, and therefore cannot form spontaneously in the thermodynamic limit of large N. For small condensates, a $j = \pm 1$ vortex may be quite likely. Several authors [46–49] had considered how such vortex states may form through stirring or rotating a condensate, but in this work it was found that there is a possibility of vortices forming spontaneously through the process of evaporative cooling. The presence of vortex states can be detected quantitatively by transforming the spatial lattice into a lattice which used the angular momentum eigenstates as a basis set. The two-dimensional results presented in Fig. 3 were obtained by integrating the spatial profile over orthogonal modes with corresponding field operators $\hat{\Psi}_{jn}$. The angular momentum distribution is then given by a summation over the radial modes,

$$n(j) = \sum_n \langle \hat{\Psi}_{jn} \hat{\Psi}^*_{jn} \rangle. \tag{15}$$

The angular momentum distribution for individual trajectories showed large occupation in particular different angular modes, indicating that vortices with different momenta appeared on each trajectory. For example, on one run a vortex with $j = -1$ appeared at about one quarter of the way through the simulation, and persisted until the end. The maximum occupation of the vortex was around $n(j) = 20$, owing to relatively small initial atom numbers in this 2D trap simulation. Shown in Fig. 3 is the ensemble average of the angular momentum distribution, which reveals quite a broad range of final angular momentum, consistent with the existence of vortices. However, it was found that the simulations could not be carried out after damping had stopped, owing to large sampling errors.

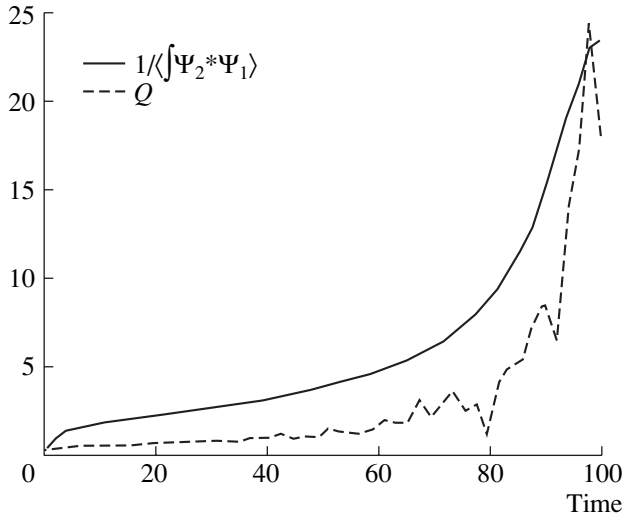

Fig. 2. Simulation of a three-dimensional Bose condensate, showing the ensemble average evolution (15 paths) of the confinement parameter Q.

4. QUANTUM SUPERCHEMISTRY

What has become known as superchemistry are processes in BEC which are analogous to the parametric nonlinear processes, such as the second and sub-harmonic generation that are well known in quantum optics. These processes between interacting bosons do not obey the usual Arrhenius rules for reaction rates because of Bose enhancement effects [12]. The processes which have been analyzed so far using mean-field models include molecular photoassociation from atomic BEC [50–53] and the potentially more robust method of molecular photoassociation via Raman-stimulated adiabatic passage [54, 55]. The process of molecular photodissociation [9] is a noise driven process and has no possible description in the mean-field approach as long as we begin with no atoms present. As demonstrated below, even the mean-field dynamics in photoassociation cannot always be described accurately by GPE equations.

4.1. Photoassociation

Photoassociation of an atomic condensate to form a molecular condensate has been investigated using a simplified mean-field model [51], while coherent molecular soliton formation has also been predicted in a similar system [11]. The mean-field dynamical behavior of atomic and molecular condensates coupled by a Raman transition has been investigated in three-dimensions, showing giant collective oscillations between the atoms and molecules [12]. This process not only produces a new species of BEC, but does it through a non-linear coupling which allows the possibility of quantum statistical effects becoming evident in the dynamics. Using the functional positive-P representation to calculate the full quantum dynamics of the atomic and molecular fields, it has been shown [8] that in certain parameter regimes the Gross–Pitaevskii equation (GPE) can give incorrect results, even for the atomic and molecular populations. This is not totally unexpected, as one of the simplest systems in quantum optics in which easily observable experimental features depend on the quantum statistics is second harmonic generation, where pairs of photons are coupled to single high-energy photons [56]. This system is mathematically analogous to molecular photoassociation and is also not accurately described by mean-field equations.

The process of two-colour Raman photoassociation is described by considering a single electronic level for the atomic field and a two-component field for the molecules. The three modes are in a Λ configuration as shown in Fig. 4, with state $|1\rangle$ being the atomic BEC, state $|2\rangle$ the excited state of the molecular condensate (MBEC) and state $|3\rangle$ the stable MBEC. The excited molecular field is actually composed of multiple vibrational levels, but these excited states are not populated by the Raman transition, so they are treated as a single level which is then adiabatically eliminated. Two separate lasers induce a free-bound coupling between $|1\rangle$ and $|2\rangle$ and a bound–bound coupling between $|2\rangle$ and $|3\rangle$. In a rotating frame, the Hamiltonian may be written as

$$\begin{aligned}\hat{H} &= \sum_{i=1}^{3}\left(\hat{T}_i + \hat{V}_i + \int d\mathbf{x}\frac{U_{ii}}{2}\hat{\psi}_i^{\dagger 2}(x)\hat{\psi}_i^2(x)\right)\\ &+ \frac{i\hbar}{2}\int d\mathbf{x}(\kappa(x)\hat{\psi}_1^{\dagger 2}(x)\hat{\psi}_2(x) - \kappa^*(x)\hat{\psi}_1^2(x)\hat{\psi}_2^\dagger(x))\\ &+ i\hbar\int d\mathbf{x}(\Omega(x)\hat{\psi}_2^\dagger(x)\hat{\psi}_3(x) - \Omega^*(x)\hat{\psi}_2(x)\hat{\psi}_3^\dagger(x)),\end{aligned} \tag{16}$$

where $\hat{\psi}_j(x)$ is the field annihilation operator for the atomic or molecular field in state $|j\rangle$, $\hat{T}_i$ and $\hat{V}_i$ are the kinetic and potential energy operators for the ith field, U_{kk} is the strength of the interatomic interactions between particles in state $|k\rangle$, $\kappa(x)$ is the Rabi frequency of the free–bound photoassociation and $\Omega(x)$ is the Rabi frequency of the bound–bound transition. The interactions between the species are not included, as the strengths are not known. In this notation, the detunings of the lasers from the bare atomic and molecular energy levels are included in the potential energy terms V_2 and V_3.

The Fokker–Planck equation resulting from the above Hamiltonian may be written as

$$\frac{\partial P}{\partial t} = \sum_{\nu}\int d\mathbf{x}\left[-\partial_\nu A^\nu + \sum_{\mu}\frac{1}{2}\partial_\mu\partial_\nu D^{\mu\nu}\right]P, \tag{17}$$

where the elements μ and ν correspond to the six components of the fields in the positive-P representation: $\{\psi_1^\alpha, \psi_1^\beta, \psi_2^\alpha, \psi_2^\beta, \psi_3^\alpha, \psi_3^\beta\}$, A is the drift vector, D is

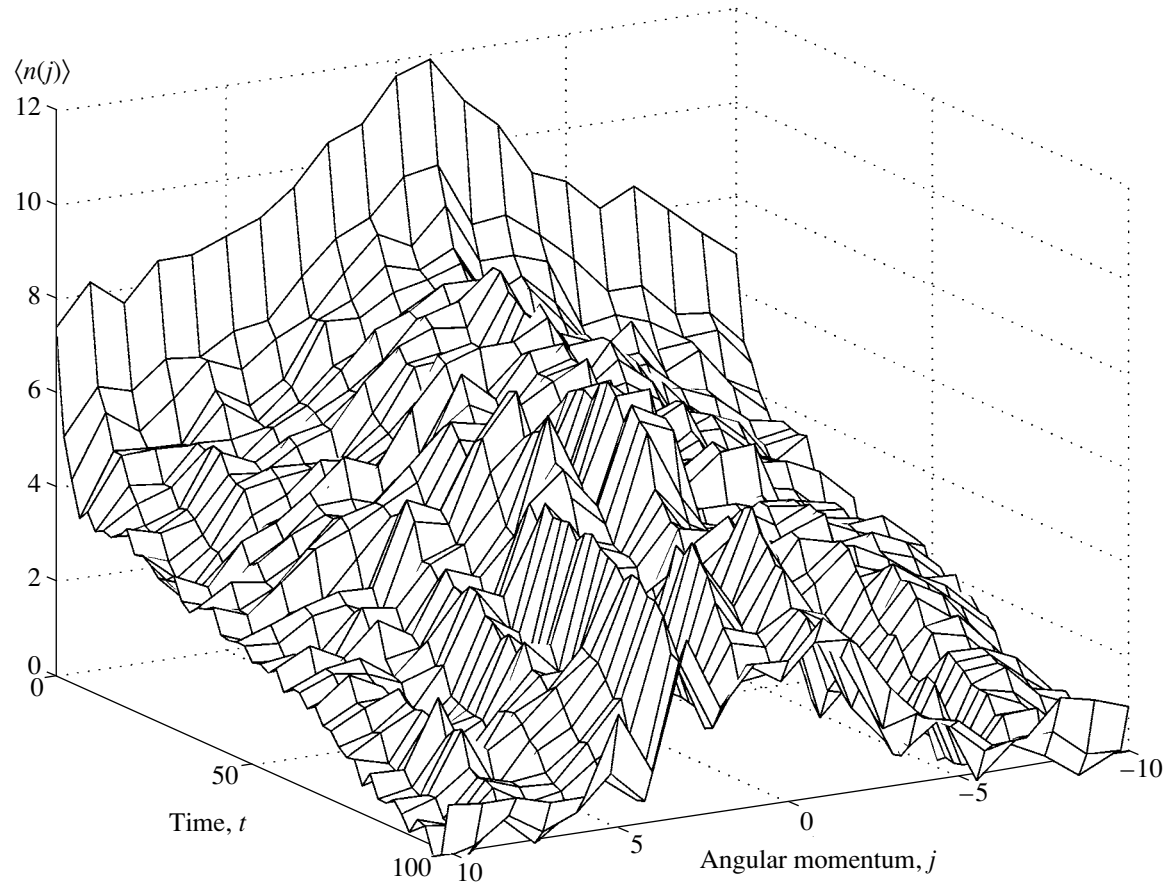

Fig. 3. Ensemble average of the angular momentum distribution $\langle n(j)\rangle$, during the condensation of a two-dimensional Bose condensate (40 paths).

the diffusion matrix, and $\partial_{(\nu \leftrightarrow \{n,\gamma\})} \equiv \dfrac{\partial}{\partial \psi_n^\gamma}$. The drift vector is given by

$$A = \begin{pmatrix} \mathcal{H}_1\psi_1^\alpha - i\Gamma_{11}\psi_1^\beta\psi_1^{\alpha 2} + \kappa\psi_1^\beta\psi_2^\alpha \\ -\mathcal{H}_1\psi_1^\beta + i\Gamma_{11}\psi_1^{\beta 2}\psi_1^\alpha + \kappa^*\psi_1^\alpha\psi_2^\beta \\ \mathcal{H}_2\psi_2^\alpha - i\Gamma_{22}\psi_2^\beta\psi_2^{\alpha 2} - \dfrac{\kappa^*}{2}\psi_1^{\alpha 2} + \Omega\psi_3^\alpha - \dfrac{\gamma}{2}\psi_2^\alpha \\ -\mathcal{H}_2\psi_2^\beta + i\Gamma_{22}\psi_2^{\beta 2}\psi_2^\alpha - \dfrac{\kappa}{2}\psi_1^{\beta 2} + \Omega^*\psi_3^\beta - \dfrac{\gamma}{2}\psi_2^\beta \\ \mathcal{H}_3\psi_3^\alpha - i\Gamma_{33}\psi_3^\beta\psi_3^{\alpha 2} - \Omega^*\psi_2^\alpha \\ -\mathcal{H}_3\psi_3^\alpha + i\Gamma_{33}\psi_3^{\beta 2}\psi_3^\alpha - \Omega\psi_2^\beta \end{pmatrix}, \quad (18)$$

where $\mathcal{H}_j = -i/\hbar(\hat{T}_j + \hat{V}_j)$, $\Gamma_{jj} = U_{jj}/\hbar$ and the damping rate of the excited molecular field is γ. The diffusion matrix D is diagonal, with diagonal elements from the vector B_{sqr}:

$$B_{\mathrm{sqr}} = \{-i\Gamma_{11}\psi_1^{\alpha 2} + \kappa\psi_2^\alpha, i\Gamma_{11}\psi_1^{\beta 2} + \kappa^*\psi_2^\beta, -i\Gamma_{22}\psi_2^{\alpha 2}, i\Gamma_{22}\psi_2^{\beta 2}, -i\Gamma_{33}\psi_3^{\alpha 2}, i\Gamma_{33}\psi_3^{\beta 2}\}. \quad (19)$$

This Fokker–Planck equation leads to the following set of Itô stochastic field equations,

$$\frac{\partial \psi_\nu}{\partial t} = A^\nu + \sqrt{B_{\mathrm{sqr}}^\nu}\,\eta_\nu, \quad (20)$$

where η_ν are a set of real δ-correlated Gaussian noise sources. These equations reduce to the GPE for this system if the noise terms are dropped.

As the single photon detuning δ must be made very large, the upper level can be adiabatically eliminated. Making the adiabatic approximation even stronger, that is assuming that the single-photon detuning δ is larger than the noise terms $\sqrt{\Gamma_{22}}\eta_{3,4}$, the excited state loss rate γ and the trapping potential ($V_2 = \hbar\delta$), then the resulting equations of motion in scaled units are

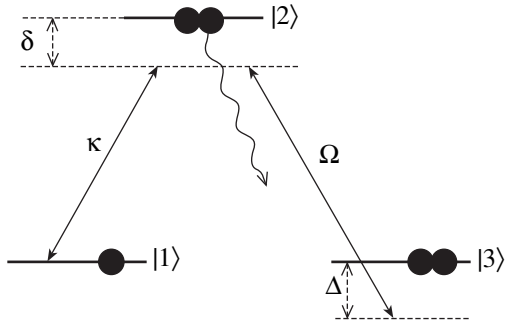

Fig. 4. Energy level scheme for coherent free-bound-bound photoassociation. Levels $|1\rangle$, $|2\rangle$, and $|3\rangle$ are the electronic states for the atomic BEC, the excited MBEC and the ground MBEC respectively.

$$\frac{\partial\psi_1^\alpha}{\partial\tau} = \tilde{\mathcal{H}}_1\psi_1^\alpha - i\Gamma_{\rm eff}\psi_1^\beta\psi_1^{\alpha 2} - i\psi_1^\beta\psi_3^\alpha + \sqrt{-i(\Gamma_{\rm eff}\psi_1^{\alpha 2} + \psi_3^\alpha)}\eta_1,$$

$$\frac{\partial\psi_1^\beta}{\partial\tau} = -\tilde{\mathcal{H}}_1\psi_1^\beta + i\Gamma_{\rm eff}\psi_1^{\beta 2}\psi_1^\alpha + i\psi_1^\alpha\psi_3^\beta + \sqrt{i(\Gamma_{\rm eff}\psi_1^{\beta 2} + \psi_3^\beta)}\eta_2,$$

$$\frac{\partial\psi_3^\alpha}{\partial\tau} = \tilde{\mathcal{H}}_3\psi_3^\alpha - i\tilde{\Gamma}_{33}\psi_3^\beta\psi_3^{\alpha 2} - \frac{i}{2}\psi_1^{\alpha 2} + i\frac{\Omega}{\kappa^*}\psi_3^\alpha + \sqrt{-i\tilde{\Gamma}_{33}}\psi_3^\alpha\eta_3,$$

$$\frac{\partial\psi_3^\beta}{\partial\tau} = -\tilde{\mathcal{H}}_3\psi_3^\beta + i\tilde{\Gamma}_{33}\psi_3^{\beta 2}\psi_3^\alpha + \frac{i}{2}\psi_1^{\beta 2} - i\frac{\Omega^*}{\kappa}\psi_3^\beta + \sqrt{i\tilde{\Gamma}_{33}}\psi_3^\beta\eta_4, \quad (21)$$

where $\chi = \kappa\Omega/\delta$, τ is the scaled time $\tau = \chi t$, $\tilde{\mathcal{H}}_j = \mathcal{H}_j/\chi$, $\tilde{\Gamma}_{jj} = \Gamma_{jj}/\chi$ and $\Gamma_{\rm eff} = \tilde{\Gamma}_{11} - \kappa/2\Omega^*$. Only four noise sources are required in this approximation.

An interesting and important aspect of this system is that there is now a nonlinear light shift of the BEC, which is proportional to κ/Ω and a linear light shift of the MBEC which is proportional to Ω/κ. By carefully selecting the ratio of the two laser intensities, the nonlinear light shift can actually cancel the repulsive interactions between the atoms. A suitable choice of the two-photon detuning Δ can then be used to make the coupling between the two stable species resonant.

The discrepancy between the semiclassically predicted dynamics and the quantum predictions in the analogous system of travelling-wave second harmonic generation with added $\chi^{(3)}$ interaction is most pronounced when there is nearly complete conversion to the second harmonic, which occurs when the third order nonlinearities are very small [57]. In the same parameter regime for conversion of a BEC to an MBEC, the sizes of both the linear and the self energy

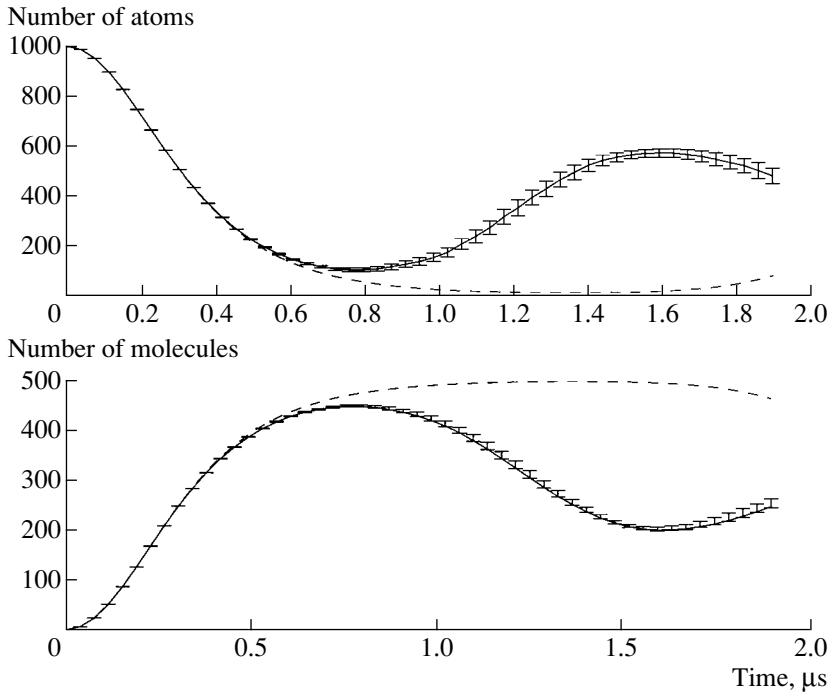

Fig. 5. Atomic and molecular populations for $\chi = 2900$ Hz m$^{1/2}$, with $\Gamma_{33} = \Gamma_{11}$. The solid line is the result of the positive-*P* calculation and the dashed line is the solution of the GPE. The error bars on the positive-*P* solution are due to the sampling error.

terms are effectively reduced. Since the atomic interactions can be balanced by light shifts, the remaining critical parameter is the intermolecular interactions. Unfortunately, there is still much uncertainty about the molecule-molecule scattering length. The results are therefore based on the assumption that the molecular scattering rate is the same as the atomic scattering rate. If it were weaker, then the difference between the positive-*P* and GPE results would be even greater.

It is experimentally difficult to produce large Rabi frequencies for the atom-molecule interaction due to the low Franck–Condon factors, but this does not appear to be a limitation of this system provided large Rabi frequencies can be achieved for the molecule-molecule transition. Figure 5 shows the evolution of the atomic and molecular populations for $\kappa = 0.29$ MHz $m^{1/2}$, $\Omega = 10$ GHz and $\delta = 100\Omega$. The mass and scattering length of ^{87}Rb were used for this calculation. Both condensates are in a quasi-1D harmonic trap of frequency $\omega/2\pi = 6.8$ Hz in the axial direction, and $\omega/2\pi = 200$ Hz in the tightly confining transverse directions. This leads to an effective interatomic repulsion of $\Gamma_{11} = 0.042$ in the one dimensional limit [6]. The stochastic integration was performed with the XMDS package [58]. Although the GPE solution exhibits a revival in atomic population, it can clearly be seen that it is inadequate for predictions over this timescale. In this process, the signature of the breakdown of the GPE approach occurs in the simplest experimental observable: the total atomic and molecular populations.

4.2. STIRAP

The more robust method of stimulated Raman adiabatic passage (STIRAP) has also been studied in a mean-field approximation [54, 55] and the quantum statistical properties of single mode STIRAP with classical electromagnetic fields and the mean-field multimode behavior in one dimension has also been studied [55]. The process of STIRAP requires a pair of overlapping laser pulses, one of which couples the BEC from the atomic state to an excited molecular state, while the other couples the excited molecular field to a stable molecular state. These pulses are applied in the *counterintuitive* sequence, where the atomic field is first exposed to the laser which couples the two molecular states. Rather than attempting to combine the atoms within the BEC to produce molecules, this laser is defining the initial state of the BEC as a *dark* state, which does not interact with the laser. As the second pulse is turned on, the dark state becomes a linear combination of the two stable states. When the first pulse is finished, the stable MBEC is in the equivalent dark state, as it is not affected by the laser which couples the atomic state to the excited molecular state. If the pulses are made sufficiently long then the system adiabatically evolves from the stable atomic BEC to the stable molecular MBEC without producing a significant population in the excited MBEC.

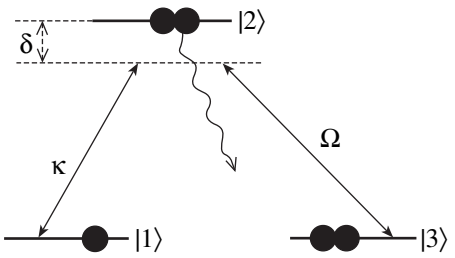

Fig. 6. Energy level scheme for coherent free-bound-bound photoassociation. Levels $|1\rangle$, $|2\rangle$, and $|3\rangle$ are the electronic states for the atomic BEC, the excited MBEC and the ground MBEC respectively.

STIRAP relies on the formation of the dark states and the ability to smoothly transfer from one to the other. Although the coupling of the atomic to molecular transition is quite weak [59], there is Bose enhancement of that transition rate, so its effective Rabi frequency can be made comparable to that of the excited-ground molecular transition, and Mackie *et al.* showed that this means that STIRAP may be a feasible method for producing an MBEC [54], although the model used ignored both the spatial structure of the condensates and the effect of the interatomic interactions. The resulting model therefore had formal similarities to travelling wave second harmonic generation [56], with the addition of an extra level. The atomic interactions introduce a term analogous to a $\chi^{(3)}$ nonlinearity, which has been known to affect the quantum statistics and dynamics in second harmonic generation [57, 60–62], therefore it was of interest to develop a more complete model.

The simplest possible model for a BEC or MBEC is to describe it as a single bosonic mode, so the STIRAP process can be described with three coupled modes [54]. This approach can give qualitative predictions as long as the times of interest are short enough. The next step up in sophistication is to include quantum noise. The three modes are in a Λ configuration as shown in Fig. 6, with state $|1\rangle$ being the atomic BEC, state $|2\rangle$ the excited state of the MBEC and state $|3\rangle$ the stable MBEC. In a rotating frame, the interaction Hamiltonian may be written as

$$\frac{\hat{H}}{\hbar} = \delta\hat{b}^\dagger\hat{b} + i\kappa[\hat{a}^{\dagger 2}\hat{b} - \hat{a}^2\hat{b}^\dagger] + i\Omega[\hat{b}^\dagger\hat{c} - \hat{b}\hat{c}^\dagger] + \chi_a\hat{a}^{\dagger 2}\hat{a}^2 + \chi_b\hat{b}^{\dagger 2}\hat{b}^2 + \chi_c\hat{c}^{\dagger 2}\hat{c}^2, \quad (22)$$

where interactions between the modes are ignored. In the above, $\hat{a}$, $\hat{b}$, and $\hat{c}$ are the annihilation operators for $|1\rangle$, $|2\rangle$, and $|3\rangle$ respectively. The couplings for the $|1\rangle \rightleftharpoons |2\rangle$ and $|2\rangle \rightleftharpoons |3\rangle$ transitions have effective strengths κ and Ω, which are time dependent.

Because the Heisenberg equations of motion for this system have no known analytic solution, the usual methods are used to derive *c*-number equations in the

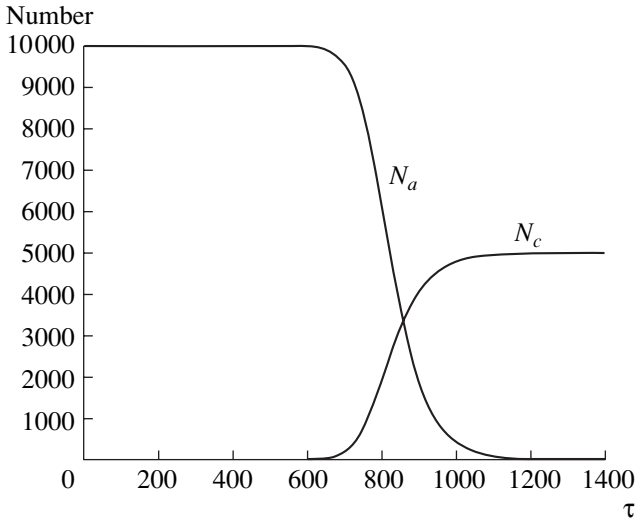

Fig. 7. The populations of N_a and N_c calculated using 10^5 stochastic trajectories. The maximum population of N_b is too small to appear at this scale. This figure does not noticeably change whether the $\chi^{(3)}$ interactions are included or not.

positive-P representation of quantum optics [63, 34], where the simplifications have been made that $\chi_a = \chi_b = \chi_c = \chi$ and $\delta = 0$,

$$\begin{aligned}
\frac{d\alpha}{dt} &= -2i\chi\alpha^2\alpha^\dagger + 2\kappa\alpha^\dagger\beta + \sqrt{2\kappa\beta - 2i\chi\alpha^2}\eta_1(t),\\
\frac{d\alpha^\dagger}{dt} &= 2i\chi\alpha^{\dagger 2}\alpha + 2\kappa\alpha\beta^\dagger + \sqrt{2\kappa\beta^\dagger + 2i\chi\alpha^{\dagger 2}}\eta_2(t),\\
\frac{d\beta}{dt} &= -2i\chi\beta^2\beta^\dagger - \kappa\alpha^2 + \Omega\gamma + \sqrt{-2i\chi\beta^2}\eta_3(t),\\
\frac{d\beta^\dagger}{dt} &= 2i\chi\beta^{\dagger 2}\beta - \kappa\alpha^{\dagger 2} + \Omega\gamma^\dagger + \sqrt{2i\chi\beta^{\dagger 2}}\eta_4(t),\\
\frac{d\gamma}{dt} &= -2i\chi\gamma^2\gamma^\dagger - \Omega\beta + \sqrt{-2i\chi\gamma^2}\eta_5(t),\\
\frac{d\gamma^\dagger}{dt} &= 2i\chi\gamma^{\dagger 2}\gamma - \Omega\beta^\dagger + \sqrt{2i\chi\gamma^{\dagger 2}}\eta_6(t),
\end{aligned} \tag{23}$$

where the real noise terms have the properties $\overline{\eta_i(t)} = 0$ and $\overline{\eta_i(t)\eta_j(t')} = \delta_{ij}\delta(t - t')$. This model ignores the spatial structure of a real condensate, although it can be considered an approximation to a one dimensional condensate in the limit where the kinetic energy term in the Hamiltonian can be ignored. In the STIRAP case this turns out to be a reasonable approximation as long as the applied fields are of short duration [55].

To solve Eq. (23), numerical stochastic integration was used, with the initial conditions that $\alpha(0) = \alpha^\dagger(0) = 100$, the values for the other two fields being zero, with the fields either in coherent states or vacuum. The applied fields, κ and Ω, were time dependent Gaussian pulses:

$$\begin{aligned}
\Omega(\tau) &= \exp\left[-\frac{1}{2}\left(\frac{\tau - T_1}{\sigma}\right)^2\right],\\
\kappa(t) &= \frac{\kappa_p}{\Omega_p}\exp\left[-\frac{1}{2}\left(\frac{\tau - T_2}{\sigma}\right)^2\right],
\end{aligned} \tag{24}$$

where Ω_p and κ_p are the peak Rabi frequencies and a dimensionless time, $\tau = \Omega_p t$, is used. The results shown in Fig. 7 were produced with the parameters $\kappa_p/\Omega_p = 0.005$, $T_1 = 533$, $T_2 = 1025$, and $\sigma = 133$, for which the stochastic integration was stable and there was a good conversion to the MBEC.

The quantities of interest are the numbers in each of the three states and the quantum statistics of the final state. As shown in Fig. 7, the mean number occupation of each mode does not change significantly with the addition of the self interaction terms. In fact, for a value $\chi = 10^{-4}$ it was found that the maximum occupation of the intermediate dark state actually decreased, from 9 with $\chi = 0$ to less than one. On the scale of the figure, there is no visible difference in the dynamics whether or not $\chi^{(3)}$ is included.

The primary interest in solving the zero dimensional model was to determine the quantum statistics of the resultant field. To this end the quadrature variances for $X_c = c + c^\dagger$ and $Y_c = -i(c - c^\dagger)$ were calculated, as well as the normalized intensity variance. Without the self-interactions, it was found that the resultant field is a little less than 50% squeezed in the X_c quadrature, as shown in Fig. 8. The field is still close to being in a minimum uncertainty state and has a normalized intensity variance indistinguishable from the variance in X_c. This is typical of resonant $\chi^{(2)}$ interactions where the mean fields remain real, as the Wigner function ellipse is squeezed but neither rotated nor moved off the X-axis. The 50% amplitude squeezing in the MBEC is a direct consequence of the fact that the process is completely converting a coherent BEC to diatomic molecules, which in the number basis simply compresses the scale of the number distribution by a factor of two.

When a non-zero $\chi^{(3)}$ component is added there is a significant difference in the quantum state of the output mode, although the dynamics are essentially unchanged. As seen in Fig. 9, while the normalized intensity variance is almost unchanged, there is now no squeezing in either quadrature. This is a signature of $\chi^{(3)}$ systems and indicates that there is a rotation and deformation of the Wigner ellipse of the initial coherent state. This effect has previously been calculated for BEC [64], showing that the contours of the Wigner function take on a banana-like shape, which can indeed give sub-Poissonian statistics at the same time as excess quadrature noise.

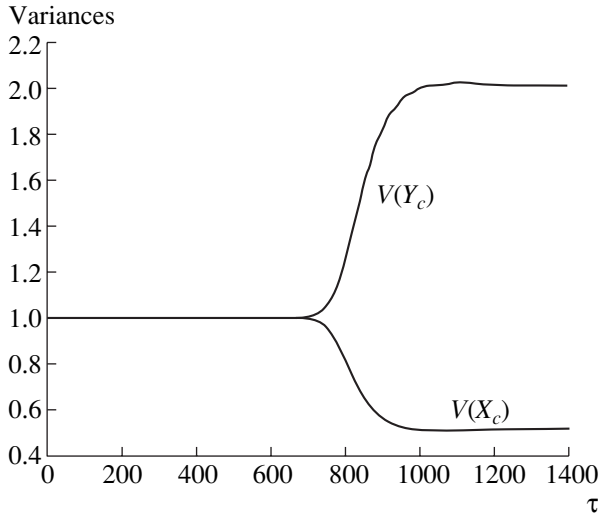

Fig. 8. The quadrature and number variances of the final state without the $\chi^{(3)}$ interaction. The final state is sub-Poissonian and squeezed in the amplitude quadrature.

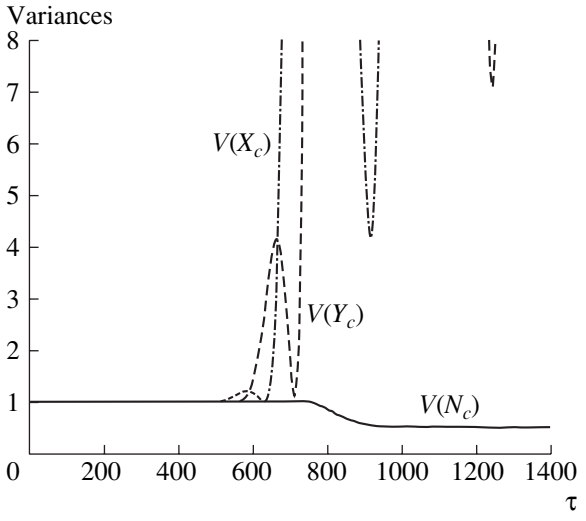

Fig. 9. The quadrature and number variances of the final state with the $\chi^{(3)}$ interaction included. The final state is sub-Poissonian but there is no steady state quadrature squeezing.

This work, and a one-dimensional semi-classical analysis by the same authors [55] demonstrated that the transfer of atoms to molecules via STIRAP was robust with respect to detunings, $\chi^{(3)}$ nonlinearities and small asymmetries between the peak strengths of the two Raman lasers—as long as the Raman laser Rabi frequencies were large enough. A complete population transfer by two short, powerful, overlapping laser pulses is possible, as long as the pulses are short on the timescale with which the kinetic energy acts. For this system, the mean-field GPE approach describes the essentials of the dynamics, but a single-mode approach which neglects the spatial structure of the problem can be misleading. Although quantum noise would not seem to affect the dynamics, the output MBEC is likely to exhibit some interesting quantum statistical features, including noise suppression effects due to the atomic combination.

5. INTRACAVITY CONDENSATE OPTICS

Another process for which a quantum description is required is that which we may call intracavity condensate optics; specifically the process of resonant photoassociation of an atomic condensate held inside an optical cavity. In the case of an intracavity electromagnetic field resonantly coupling atomic and molecular Bose–Einstein condensates (BEC), it has been shown that a photon blockade effect can be caused and that the dynamics of the three fields are not even qualitatively similar to those of mean-field predictions [65]. The effects described are not present for a travelling wave electromagnetic field interacting with the condensate, but occur because of correlations that build up between the matter fields and the confined electromagnetic field. Although there are parametric processes in nonlinear optics where the noise properties are also important in the dynamics, the system described here exhibits a richer range of behaviors because the quantization of the electromagnetic field means that we effectively have a quantized $\chi^{(2)}$ nonlinearity, which is not possible with optical parametric systems.

Methods have been developed to study the interaction of quantized matter and electromagnetic fields [66–68], although these have only been applied after making various approximations, including linearization of the resulting equations of motion. As the system of photoassociation considered here has formal similarities to SHG and behavior has been predicted there that is not calculable in a mean-field, or linearized, approximation [56], it is better to use the phase space methods of quantum optics.

The system considered is as shown schematically in Fig. 10. A trapped atomic condensate is held in an electromagnetic cavity. The empty cavity is resonant at the frequency of the transition between atomic and molecular states of the condensate. The approximation is made that all three fields can be represented as single modes, which is reasonable as long as we are considering short interaction times where the kinetic energy may be ignored [55]. Spontaneous dissociation of the molecules is also ignored, again because the interesting physics happens on a short timescale. The vibrational and rotational levels of the molecular state can also be ignored, as long as the energy spacing between these is more than the laser linewidth.

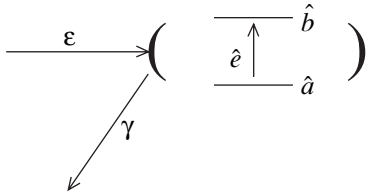

Fig. 10. Schematic of the condensate, represented by the operators $\hat{a}$ and $\hat{b}$, inside the electromagnetic cavity with field operator $\hat{e}$. The classical cavity pumping is represented by ϵ and the loss rate is represented by γ.

The interaction Hamiltonian for this system in the rotating wave approximation is

$$\begin{aligned}\mathcal{H} &= \frac{i\hbar g}{2}[\hat{a}^{\dagger 2}\hat{b}\hat{e}^{\dagger} - \hat{a}^{2}\hat{b}^{\dagger}\hat{e}] \\ &+ \hbar\chi_a\hat{a}^{\dagger 2}\hat{a}^{2} + \hbar\chi_b\hat{b}^{\dagger 2}\hat{b}^{2} \\ &+ i\hbar(\epsilon\hat{e}^{\dagger} - \epsilon^{*}\hat{e}) \\ &+ \Gamma^{\dagger}\hat{e} + \Gamma\hat{e}^{\dagger},\end{aligned} \tag{25}$$

where g represents the effective coupling strength between the condensates and the electromagnetic field, $\hat{a}(\hat{b})$ is the annihilation operator for the atomic (molecular) condensate and $\hat{e}$ is the annihilation operator for the intracavity electromagnetic field. The χ_j represent the self-interaction terms between the atoms or molecules, ϵ represents the classical pumping of the cavity and Γ is a bath operator for the electromagnetic field.

Following the standard methods [34], a partial differential equation for the P distribution of this system can be derived, which does, however, contain third-order derivatives. An approximation which is commonly made, especially in the Wigner representation, is to truncate the equation at second order. This has been shown to be accurate for the dynamics and quadrature variances of second harmonic generation [56] and for calculating first order correlation functions in trapped BEC [6], although it is not accurate for the calculation of higher order correlations in travelling wave SHG [69, 70]. This truncation can be justified by claiming that the coefficients of the third order terms are smaller than the other coefficients in the equation, which is certainly the case in this example. After truncation, the following set of Itô stochastic differential equations in the positive-P representation are found

$$\begin{aligned}\frac{d\alpha}{dt} &= -2i\chi_a\alpha^{\dagger}\alpha^{2} + ge^{\dagger}\alpha^{\dagger}\beta + \frac{\sqrt{g}}{2}(e^{\dagger}+\beta)\eta_1(t) \\ &+ \frac{i\sqrt{g}}{2}(e^{\dagger}-\beta)\eta_3(t) + \sqrt{-2i\chi_a\alpha^{2}}\eta_5(t), \\ \frac{d\alpha^{\dagger}}{dt} &= 2i\chi_a\alpha^{\dagger 2}\alpha + ge\alpha\beta^{\dagger} + \frac{\sqrt{g}}{2}(e+\beta^{\dagger})\eta_2(t) \\ &- \frac{i\sqrt{g}}{2}(e-\beta^{\dagger})\eta_4(t) + \sqrt{2i\chi_a\alpha^{\dagger 2}}\eta_6(t), \\ \frac{d\beta}{dt} &= -2i\chi_b\beta^{2}\beta^{\dagger} - \frac{g}{2}\alpha^{2}e + \sqrt{-2i\chi_b\beta^{2}}\eta_7(t), \\ \frac{d\beta^{\dagger}}{dt} &= 2i\chi_b\beta^{\dagger 2}\beta - \frac{g}{2}\alpha^{\dagger 2}e^{\dagger} + \sqrt{2i\chi_b\beta^{\dagger 2}}\eta_8(t), \\ \frac{de}{dt} &= \epsilon - \gamma e + \frac{g}{2}\alpha^{\dagger 2}\beta + \sqrt{g}\alpha^{\dagger}\eta_1(t) + i\sqrt{g}\alpha^{\dagger}\eta_3(t), \\ \frac{de^{\dagger}}{dt} &= \epsilon^{*} - \gamma e^{\dagger} + \frac{g}{2}\alpha^{2}\beta^{\dagger} + \sqrt{g}\alpha\eta_2(t) - i\sqrt{g}\alpha\eta_4(t),\end{aligned} \tag{26}$$

where the real noise sources have the properties

$$\overline{\eta_i(t)} = 0, \quad \overline{\eta_j(t)\eta_k(t')} = \delta_{jk}\delta(t-t'). \tag{27}$$

We note here that it is possible to write the noise terms in many different ways, amounting to different factorizations of the diffusion matrix.

We have solved Eq. (26) numerically for a range of parameters, finding behavior of the mean fields that is strikingly different from that found in the usual mean-field approximation. This is completely different from many situations in quantum optics or in the study of condensates, where the dynamics of the mean fields can be successfully described by considering only the drift terms in the appropriate Fokker–Planck equation.

The simulations were begun with an atomic condensate inside a cavity which begins to be pumped at $t = 0$. Initially neither molecules nor electromagnetic field are present, with the atomic field being treated as being initially in a coherent state. It was found that this system exhibits at least three regimes of behavior, only one of which is described in detail here. The behavior shown in the plots comes from what may be considered the strong-interaction regime and always exhibits short-time oscillations and photon blockade [71, 72]. In the weak-interaction regime, which may be reached by decreasing the strength of g or the number of atoms, the solutions approach those found by treating all fields semiclassically. In this case the solutions for atom and molecule number are similar to those found in superchemistry [12]. There are almost total oscillations between the two states and the photon blockade is not seen. There is also a regime between these two in which there are no oscillations, but partial conversion between atoms and molecules, with the photon blockade effect being seen as the conversion stops.

Figure 11 is shown the time development of the atomic and molecular fields as the cavity is turned on, for the parameters $g = 10^{-5}$, $|\epsilon|^2 = 10^6$, $\chi_{a,b} = 10^{-9}$, and $|\alpha(0)|^2 = 10^6$, which are all scaled in terms of the cavity loss rate. The means were taken over 5×10^5 stochastic

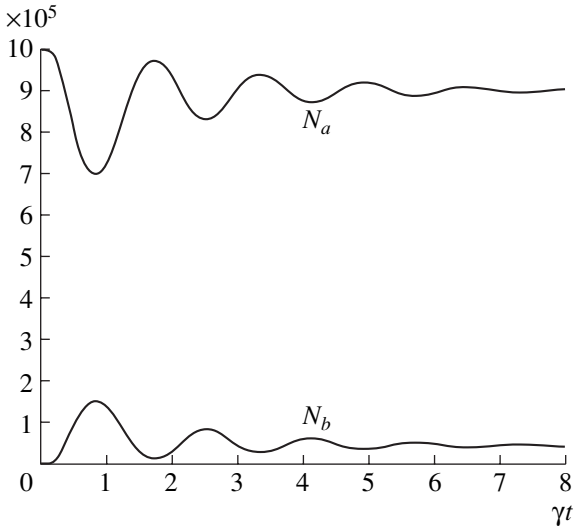

Fig. 11. Occupation numbers of the atomic and molecular condensates as a function of time according to 5×10^5 quantum trajectories. The parameters are $g = 10^{-5}$, $|\epsilon|^2 = 10^6$, $\chi_{a,b} = 10^{-9}$, and $|\alpha(0)|^2 = 10^6$. In all graphs, the quantities are dimensionless.

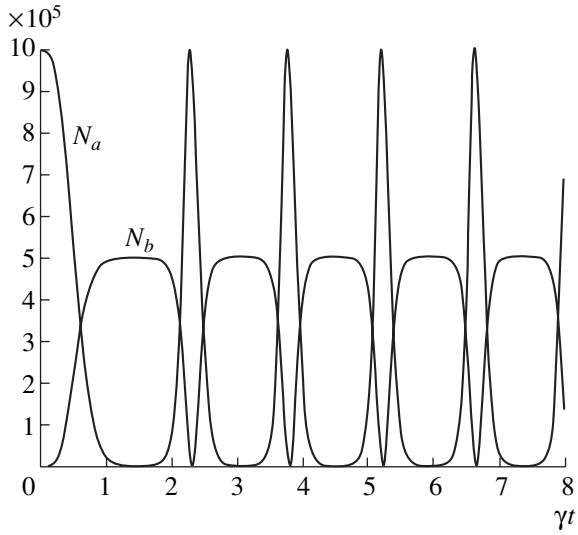

Fig. 12. Linearized solutions for the occupation numbers of the atomic and molecular condensates as a function of time.

trajectories, which was sufficient to ensure excellent convergence. What is seen is that the atoms begin to associate to form molecules, but that only a small fraction are converted before the system undergoes transient oscillations between its atomic and molecular components. After a few cavity lifetimes, both components reach a steady-state, with over 90% of the population still being in the atomic state. Of course this steady state only exists in the absence of spontaneous dissociation of the condensed molecules into non-condensed modes.

It is instructive to consider the linearized solutions for the mean-fields, i.e., the solutions of Eq. (26) with the noise terms removed, treating all three fields semiclassically. Because of the dependence of the noise terms on all three fields, it is not sensible here to treat, for example, the matter fields quantum mechanically and the electromagnetic field semiclassically.

However, when these solutions are examined, it can be seen from Fig. 12 that after approximately the first third of a cavity lifetime, they do not even approximate the quantum solutions. This disagreement is even more striking than that previously found for pure travelling-wave SHG [56] and can be qualitatively explained as the result of correlations that build up between the three fields. Some insight into the reason for this unexpected behavior can be gained when the dynamics of the intracavity electromagnetic field are examined, as shown in Fig. 13. An initial build up of intensity is seen in the cavity, with this field also becoming oscillatory and eventually almost vanishing completely. As the cavity continues to be pumped at the same rate, what is seen is that it has become opaque. That is, a photon blockade effect is operating, due to correlations which build up between the electromagnetic and matter fields [71, 72]. This effect has been seen previously in systems which develop an effective giant $\chi^{(3)}$ nonlinearity. In the linearized approach, the electromagnetic field rises monotonically to a steady state value very close to $|\epsilon|^2/\gamma$, as shown in Fig. 13, in stark contrast to the effectively empty cavity of the quantum solutions. What can be seen here is that even going one step past the usual approach, which has treated the field–matter coupling as constant, and linearizing the quantum equations, which maintains to some degree the dynamics of the effective interaction, is not enough to give the correct solutions.

5.1. Truncated Wigner Approach

A semiclassical approach that is often used in quantum optics is the theory of stochastic electrodynamics [10], usually in the guise of linearized operator equations or a truncated Wigner representation. This has also been applied to BEC [6], giving results consistent with the positive-*P* in that work. This theory is semiclassical in the sense that it locally real and seeks to explain phenomena using classical evolution under the influence of vacuum fluctuations. By definition, it cannot describe processes requiring a negative Wigner function. However, use of the truncated Wigner stochastic differential equations for BEC has significant advantages over the positive-*P* in terms of the numerical stability of the integration. In a real sense it also allows a distinction to be made between processes and effects that are truly quantum and those which have a possible semiclassical description.

It is interesting to compare the truncated Wigner predictions for intracavity photoassociation with those

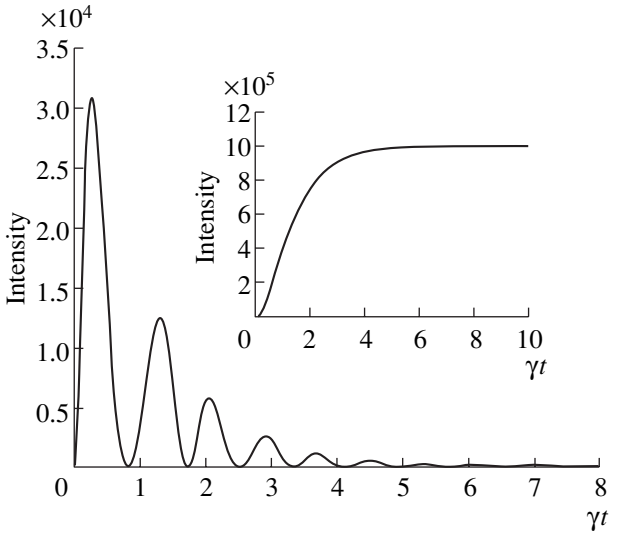

Fig. 13. The intracavity intensity of the electromagnetic field as calculated quantum mechanically, showing the photon blockade. The semiclassical solution is shown in the insert and rises to a value of almost 10^6.

of the positive-*P*, which itself needed truncation for this system. From the Hamiltonian of Eq. (25) we may use operator correspondences to find a partial differential equation for the Wigner distribution [34], which may then be truncated and mapped onto the following coupled stochastic partial differential equations for α, β, and e

$$\frac{d\alpha}{dt} = -2i\chi_a|\alpha|^2\alpha + ge^*\alpha^*\beta,$$
$$\frac{d\beta}{dt} = -2i\chi_b|\beta|^2\beta - \frac{g}{2}\alpha^2 e, \qquad (28)$$
$$\frac{de}{dt} = \epsilon - \gamma e + \frac{g}{2}\alpha^{*2}\beta + \sqrt{\frac{\gamma}{2}}[\xi_1(t) + i\xi_2(t)],$$

where the ξ_j are independent real Gaussian noise sources of unit strength.

This set of equations can also be integrated numerically, with the same initial conditions and parameters as in Section 5, with the proviso that the initial conditions are represented by their Wigner distributions. What we find is that the results for the mean fields are indistinguishable from those obtained using a truncated positive-*P*. This gives an indication that the difference between the quantum solutions and the semi-classical solutions is not due to any deeply quantum properties of the system, but can be explained by the semiclassical/semi-quantum number fluctuations of the zero point fields. By definition, the fact that these same solutions occur in the truncated Wigner gives an indication that the Wigner function for this system remains positive, which can be taken as a definition of semi-classical behavior. It is still an open question what effects may result from the third-order terms which were dropped to give the positive-*P* equations, although other results show that these have no observable effect on the mean fields [73]. There remains the possibility that the different representations will predict different values for some correlation functions, as in travelling wave second harmonic generation [70], although this is beyond the scope of this article.

6. ANALYTICAL ASYMPTOTIC SOLUTIONS

Mean field behavior of a trapped BEC which is not calculable via the standard GPE can also be found using asymptotic self-similar solutions to the GPE [74, 75] and thus obtaining a semiclassical Hamiltonian which lends itself to quantization [76]. This method extends previous results found for the case of pulse amplification in a single-mode optical fiber [77]. The process begins with the Gross–Pitaevskii gain equation [75, 78] normalized to the number, N_c, of condensed atoms

$$i\frac{\partial\psi}{\partial t} = \left(\frac{-\hbar\nabla^2}{2m} + \sum_{k=1}^{3}\frac{m\omega_k^2 x_k^2}{2\hbar} + \frac{4\pi\hbar a_s}{m}|\psi|^2 + \frac{ig(t)}{2}\right)\psi, \qquad (29)$$

where all terms have their usual meanings and the gain function is determined by the logarithmic derivative

$$g(t) = \frac{d}{dt}\log N_c(t). \qquad (30)$$

Equation (29) has asymptotic and self-similar solutions [75] for large positive values of the dimensionless parameter

$$E_c = 8\pi n_c a_s l_m^2, \qquad (31)$$

where l_m is the minimum length along one of the three axes and n_c is the average density. By writing the wavefunction with a real amplitude and phase,

$$\psi(\mathbf{x}, t) = A(\mathbf{x}, t)\exp[i\phi(\mathbf{x}, t)], \qquad (32)$$

the solution for the amplitude can be found as

$$A(\mathbf{x}, t) = \left(\frac{15}{8\pi}\right)^{1/2}\left[\frac{N_c(t)}{a_1(t)a_2(t)a_3(t)}\right]^{1/2}F(\mathbf{x}, t), \qquad (33)$$

where a_k are the ellipsoidal parameters of the BEC and

$$F(\mathbf{x}, t) = \left[1 - \sum_{k=1}^{3}\frac{x_k^2}{a_k^2(t)}\right]^{1/2}, \qquad (34)$$

where this is real and positive, and zero otherwise. The phase variable is defined by the functions $\phi_0(t)$ and $c_k(t)$ by the relation

$$\phi(\mathbf{x}, t) = \phi_0(t) + \sum_{k=1}^{3}c_k(t)x_k^2, \qquad (35)$$

where

$$c_k(t) = \frac{m}{2\hbar}\frac{d}{dt}\log a_k(t), \tag{36}$$

so that

$$\phi_0(t) = \phi_0(0) - \frac{15\hbar a_s}{2m}\int_0^t \frac{N_c(t')dt'}{a_1(t')a_2(t')a_3(t')}. \tag{37}$$

The ellipsoidal parameters are solutions of the equations

$$\frac{d^2}{dt^2}a_k + \omega_k^2 a_k = \left(\frac{15a_s\hbar^2}{m^2}\right)\frac{N_c(t)}{a_1a_2a_3a_k}, \tag{38}$$

with initial conditions $a_k(0)$ and

$$\left.\frac{da_k}{dt}\right|_{t=0} = \frac{2\hbar}{m}c_k(0)a_k(0), \tag{39}$$

which shows that there is an oscillation in the elliptical parameters. An important property of these equations is that they show how the gain process allows oscillatory center-of-mass motion to survive undamped, while condensate continues to grow. This behavior is also observed in the first-principles evaporative cooling simulations [7] and may well be of great importance for continuous-wave atom lasers.

7. CONCLUSION

We have analyzed a number of cases where BEC dynamics are not accurately predicted by solution of the Gross–Pitaevskii equation. One of these, evaporative cooling, does not even have a possible description via mean-field equations, as it begins with an ensemble of non-condensed atoms. For the other situations, while the GPE approach gives predictions, for many parameter regimes these are qualitatively wrong. In the superchemistry processes, this error shows up in the simplest possible observables; that is, in the atomic and molecular populations. In cavity photoassociation the signature of these quantum effects is also easily seen in the intensity of the intracavity electromagnetic field. What this work shows is that a trapped BEC is indeed a quantum creature and that much care must be taken with dynamical calculations, even when we do not wish to find information about the quantum statistics.

ACKNOWLEDGMENTS

This research was supported by the Marsden Fund of the Royal Society of New Zealand, the Australian Research Council and the IREX Project of the Australian Research Council. Murray Olsen wishes to thank the Physics Department of the University of Queensland for generous hospitality.

REFERENCES

1. Bose, S.N., 1924, *Z. Phys.*, **26**, 178.
2. Einstein, A., 1924, *Sitzungsber. K. Preuss. Akad. Wiss.*, 261.
3. Einstein, A., 1925, *Sitzungsber. K. Preuss. Akad. Wiss.*, 3.
4. Andersen, M.H., Ensher, J.R., Matthews, M.R., *et al.*, 1995, *Science*, **269**, 198.
5. Dalfovo, F., Giorgini, S., Pitaevskii, L.P., and Stringari, S., 1999, *Rev. Mod. Phys.*, **71**, 463.
6. Steel, M.J. *et al.*, 1998, *Phys. Rev. A*, **58**, 4824.
7. Drummond, P.D. and Corney, J.F., 1999, *Phys. Rev. A*, **60**, R2661.
8. Hope, J.J. and Olsen, M.K., 2001, *Phys. Rev. Lett.*, **86**, 3220.
9. Poulsen, U.V. and Mølmer, K., 2001, *Phys. Rev. A*, **63**, 023604.
10. Marshall, T.W., 1963, *Proc. R. Soc. London, Ser. A*, **276**, 475.
11. Drummond, P.D., Kheruntsyan, K.V., and He, H., 1998, *Phys. Rev. Lett.*, **81**, 3055.
12. Heinzen, D.J. *et al.*, 2000, *Phys. Rev. Lett.*, **84**, 5029.
13. Holland, M., Park, J., and Walser, R., 2001, *Phys. Rev. Lett.*, **86**, 1915.
14. Bogoliubov, N.N., 1947, *J. Phys.* (Moscow), **11**, 23.
15. Huang, K. and Yang, C.N., 1957, *Phys. Rev.*, **105**, 767; Huang, K., Yang, C.N., and Luttinger, J.M., 1957, *Phys. Rev.*, **105**, 776.
16. Beliaev, S.T., 1958, *Sov. Phys. JETP*, **34**, 289.
17. Fetter, A.L. and Walecka, J.D., 1991, *Quantum Theory of Many-Particle Systems* (New York: McGraw-Hill); Abrikosov, A.A., Gorkov, L.P., and Dzyaloshinski, I.E., 1963, *Methods of Quantum Field Theory in Statistical Physics* (New York: Dover).
18. Proukakis, N.P., Burnett, K., and Stoof, H.T.C., 1998, *Phys. Rev. A*, **57**, 1230; Zaremba, E., Griffin, A., and Nikuni, T., 1998, *Phys. Rev. A*, **57**, 4695.
19. Lieb, E.H. and Liniger, W., 1963, *Phys. Rev.*, **130**, 1605, 1616.
20. Krauth, W., 1996, *Phys. Rev. Lett.*, **77**, 3695.
21. Feynman, R.P., 1982, *Int. J. Theor. Phys.*, **21**, 467.
22. Wright, E.M., Walls, D.F., and Garrison, J.C., 1996, *Phys. Rev. Lett.*, **77**, 2158.
23. Carter, S.J. *et al.*, 1987, *Phys. Rev. Lett.*, **58**, 1841.
24. Drummond, P.D. and Carter, S.J., 1987, *J. Opt. Soc. Am. B*, **4**, 1565.
25. Friberg, S.R. *et al.*, 1996, *Phys. Rev. Lett.*, **77**, 3775.
26. Werner, M.J., 1996, *Phys. Rev. A*, **54**, R2567.
27. Shelby, R.M. *et al.*, 1986, *Phys. Rev. Lett.*, **57**, 691.
28. Spälter, S. *et al.*, 1997, *Europhys. Lett.*, **38**, 335.
29. Andrews, M.R. *et al.*, 1997, *Science*, **275**, 637.
30. Mewes, M.-O. *et al.*, 1997, *Phys. Rev. Lett.*, **78**, 582.
31. Drummond, P.D. and Gardiner, C.W., 1980, *J. Phys. A*, **13**, 2353.
32. Graham, R. and Haken, H., 1970, *Z. Phys.*, **234**, 193.
33. Graham, R. and Haken, H., 1970, *Z. Phys.*, **235**, 166.
34. Gardiner, C.W., 1991, *Quantum Noise* (Berlin: Springer).

35. Kennedy, T.A.B. and Wright, E.M., 1988, *Phys. Rev. A*, **38**, 212.
36. Drummond, P.D. and Hardman, A.D., 1993, *Europhys. Lett.*, **21**, 279.
37. Carusotto, I., Castin, Y., and Dalibard, J., 2001, *Phys. Rev. A*, **63**, 023606.
38. Deuar, P. and Drummond, P.D., 2001, *Commun. Comp. Phys.* (in press).
39. Plimak, L.I., Olsen, M.K., and Collett, M.J., 2001, *Phys. Rev. A*, **64**, 025801.
40. Gardiner, C.W. and Zoller, P., 2000, *Phys. Rev. A*, **61**, 033601; Lee, M.D. *et al.*, 2000, *Phys. Rev. A*, **62**, 033606.
41. Stoof, H.T.C., 1997, *Phys. Rev. Lett.*, **78**, 768.
42. Kagan, Yu.M., Svistunov, B.V., and Shlyapnokov, G.V., 1994, *Sov. Phys. JETP*, **78**, 187.
43. Zurek, W.H., 1985, *Nature*, **317**, 505.
44. Carter, S.J. *et al.*, 1987, *Phys. Rev. A*, **58**, 1841.
45. Hall, M.J.W., 1999, *Phys. Rev. A*, **59**, 2602.
46. Marzlin, K.-P., Zhang, W., and Wright, E.M., 1997, *Phys. Rev. Lett.*, **79**, 4728.
47. Dodd, R.J., Burnett, K., Edwards, M., and Clark, C.W., 1997, *Phys. Rev. A*, **56**, 587.
48. Edwards, M. *et al.*, 1996, *Phys. Rev. A*, **53**, R1950.
49. Sinha, S., 1997, *Phys. Rev. A*, **55**, 4325.
50. Julienne, P.S. *et al.*, 1998, *Phys. Rev. A*, **58**, R797.
51. Javanainen, J. and Mackie, M., 1999, *Phys. Rev. A*, **59**, R3186.
52. Javanainen, J. and Kŏstrun, M., 1999, *Opt. Express*, **5**, 188.
53. Kŏstrun, M. *et al.*, 2000, *Phys. Rev. A*, **62**, 063616.
54. Mackie, M., Kowalski, R., and Javanainen, J., 2000, *Phys. Rev. Lett.*, **84**, 3803.
55. Hope, J.J., Olsen, M.K., and Plimak, L.I., 2001, *Phys. Rev. A*, **63**, 043603.
56. Olsen, M.K. *et al.*, 2000, *Phys. Rev. A*, **61**, R021803.
57. Olsen, M.K., Kruglov, V.I., and Collett, M.J., 2001, *Phys. Rev. A*, **63**, 033801.
58. Collecutt, G.R., Drummond, P.D., and He, H., http://www.physics.uq.edu.au/xmds/.
59. Javanainen, J. and Mackie, M., 1998, *Phys. Rev. A*, **58**, R789.
60. Cabrillo, C. and Bermejo, F.J., 1992, *Phys. Lett. A*, **170**, 300.
61. Kheruntsyan, K.V. *et al.*, 1997, *Opt. Commun.*, **139**, 157.
62. Cabrillo, C., Roldán, J.L., and García-Fernandez, P., 1997, *Phys. Rev. A*, **56**, 5131.
63. Drummond, P.D. and Gardiner, C.W., 1980, *J. Phys. A*, **13**, 2353.
64. Dunningham, J.A., Collett, M.J., and Walls, D.F., 1998, *Phys. Lett. A*, **245**, 49.
65. Olsen, M.K., Hope, J.J., and Plimak, L.I., 2001, *Phys. Rev. A*, **64**, 013601.
66. Marzlin, K-P. and Audretsch, J., 1998, *Phys. Rev. A*, **57**, 1333.
67. Moore, M.G., Zobay, O., and Meystre, P., 1999, *Phys. Rev. A*, **60**, 1491.
68. Krutitsky, K.V., Burgbacher, F., and Audretsch, J., 1999, *Phys. Rev. A*, **59**, 1517.
69. Olsen, M.K. *et al.*, 2000, *Phys. Rev. A*, **62**, 023802.
70. Olsen, M.K., Plimak, L.I., and Dechoum, K., 2001, *Opt. Commun.*, **190**, 261.
71. Rebić, S., Tan, S.M., Parkins, A.S., and Walls, D.F., 1999, *J. Opt. B: Quantum Semiclassic. Opt.*, **1**, 490.
72. Werner, M.J. and Imamoğlu, A., 1999, *Phys. Rev. A*, **61**, 011801.
73. Olsen, M.K., Plimak, L.I., and Collett, M.J., 2001, *Phys. Rev. A*, **64**, 063601.
74. Fermann, M.E. *et al.*, 2000, *Phys. Rev. Lett.*, **84**, 6010.
75. Drummond, P.D. and Kheruntsyan, K.V., 2001, *Phys. Rev. A*, **63**, 013605.
76. Kruglov, V.I., Olsen, M.K., and Collett, M.J. (in preparation).
77. Kruglov, V.I. *et al.*, 2000, *Opt. Lett.*, **25**, 1753.
78. Kneer, B. *et al.*, 1998, *Phys. Rev. A*, **58**, 4841.